Materials Science and Engineering A 527 (2010) 7115–7125

Contents lists available at ScienceDirect

Materials Science and Engineering A

journal homepage: www.elsevier.com/locate/msea

Grain boundary characterization and energetics of superalloys

Michael D. Sangid[a], Huseyin Sehitoglu[a,*], Hans J. Maier[b], Thomas Niendorf[b]

[a] Department of Mechanical Science and Engineering, University of Illinois at Urbana-Champaign, 1206 West Green Street, Urbana, IL 61801, USA
[b] Lehrstuhl für Werkstoffkunde (Materials Science), University of Paderborn, 33095 Paderborn, Germany

ARTICLE INFO

Article history:
Received 27 May 2010
Accepted 17 July 2010

Keywords:
Molecular dynamics simulations
Coincidence site lattice (CSL)
Grain boundary energy
Nickel-based superalloys
Electron back scattering diffraction (EBSD)

ABSTRACT

In many engineering alloys, there exists a wide distribution of grain sizes; we investigate the role of grain boundaries as a strengthening mechanism in such a material. The coincidental site lattice (CSL) model is a powerful mathematical tool to characterize grain boundaries (GBs) and identify 'special' boundaries, which display beneficial mechanical behavior. We define the CSL and describe a detailed procedure to obtain this information from the grain orientation mapping via electron back scattering diffraction (EBSD). From this information, we show the evolution of the CSL for a nickel-based superalloy, Udimet 720 (U720), throughout various stages of processing (billet and forging) and experiments (tension, compression, and fatigue). A deeper level of understanding the GB's role in the mechanical behavior of the material is investigated through atomic simulations using molecular dynamics (MD) as the GB energy is determined for the most prevalent GBs within this material. The spatial map of the orientation and grain sizes measured from EBSD is linked to the GB energies calculated from MD. Based upon the large number of boundaries analyzed (29,035), there is a strong inverse correlation between GB energy and grain size for every specimen examined during the various processing and testing conditions.

© 2010 Elsevier B.V. All rights reserved.

1. Introduction

It is well established that grain boundaries (GBs) have a significant effect on mechanical behavior [1]. Grain boundaries offer a strengthening mechanism, as finer grains have a greater number of grain boundaries per volume. Historically, three explanations of the GB strengthening mechanism were published. Hall and Petch stated that smaller grains lead to more dislocation pile-ups resulting in stress concentration that activates dislocation sources in neighboring grains [2,3]. Ashby's dislocation interaction model contended smaller grains resulted in the mean free path for dislocations decreasing leading to more dislocation interactions and an increase in work-hardening [4]. Li and Chou argued that GBs can act as sources for dislocations thus further contributing to hardening behavior [5]. As a result, finer grain materials exhibit greater yield [1–3], fracture [1,6,7], and fatigue [8–14] strength than coarse grain material. These grain size relations are based on a homogeneous microstructure, although in real materials, there exists a grain size distribution. Hence, one needs to analyze a distribution of grain sizes to understand their effect on engineering materials. In one such study, using a self-consistent, elastic–viscoplastic model, Berbenni et al. have shown that the yield strength decreases with increasing deviation from a nominal grain size [15]. In this paper, we analyze grain boundaries from a wide distribution of grain sizes and investigate their potential role as a strengthening mechanism.

To gain a deeper understanding of the role of GBs, their structure must be characterized. A grain boundary involves two adjacent grains connected by an interface, as shown in Fig. 1a. By including the nature of the grain boundary, one can model GBs as lattice rotations of type: twist (axis of rotation is parallel to the normal of the GB, Fig. 1b), tilt (axis of rotation is perpendicular to the GB normal, Fig. 1c), or mixed. It should be expected that a certain number of the atoms in each lattice have coincidental locations from one grain to the next. This is known as a coincidental site lattice, CSL. Further, special grain boundaries come as a consequence of the CSL, by taking the reciprocal of the fraction of coincidental sites; one can obtain the CSL Σ value. Fig. 2 shows the atomic configuration of a grain boundary, in this case, a twin, where the lattices are tilted 109.47° about the ⟨1 1 0⟩ axis. Layer 0 represents the GB, where the atoms are mirrored about this twin plane. The stacking sequence moving away from the GB is C (red), B (silver), A (blue) in both grains. By looking normal to the GB, we see the top grain and bottom grain (Fig. 2, right) both display the same A, C, B stacking, although the B and C atoms have inverted locations. Hence, now one out of the three atoms are in coincidental sites across the GB, since only the A atoms align from one grain to the next. By taking the reciprocal of the number of coincidental site atoms, we obtain the CSL Σ value, which in this case is denoted as a $\Sigma 3$ GB (all twins are $\Sigma 3$ GBs). Further special grain boundaries come as a consequence of the CSL. Fig. 3 shows the same GB from a different perspective. We see

* Corresponding author. Tel.: +1 217 333 4112; fax: +1 217 244 6534.
E-mail addresses: huseyin@illinois.edu, huseyin@uiuc.edu (H. Sehitoglu).

0921-5093/$ – see front matter © 2010 Elsevier B.V. All rights reserved.
doi:10.1016/j.msea.2010.07.062

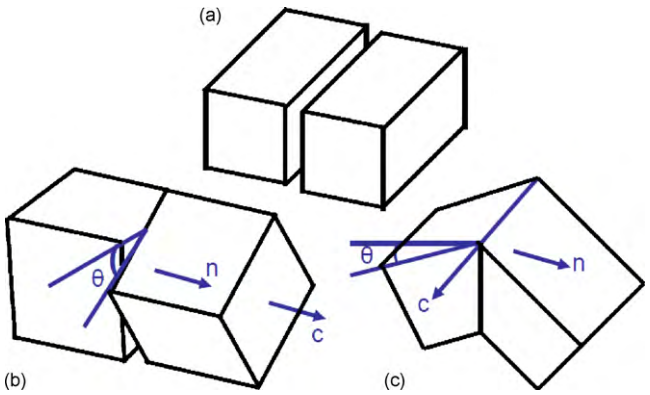

Fig. 1. (a) Schematic of two adjacent lattices, where the interface is known as a grain boundary (GB), (b) a twist GB as the axis of rotation corresponds to the normal plane of the GB, (c) a tilt GB as the axis of rotation is perpendicular to the GB normal.

a group of atoms (bottom) that are in perfect agreement with the supercell background, the (1 1 1) plane. By taking a 60° twist rotation about the (1 1 1) plane, the ordering of the atoms are deviated such that once again the red and silver atoms do not align with the background lattice, thus one out of three atoms are in coincidental lattice locations denoting the Σ3 GB.

In 1949, Kronberg and Wilson [16] were the first to point out the importance of the CSL to mechanical properties. They observed coincidence patterns in the boundary planes, which in the present CSL theory corresponds to Σ7 and Σ13 GBs. Kronberg and Wilson noted the significance of low Σ values for nucleation and growth during secondary recrystallization of copper as they found less segregation existing in these low Σ boundaries. More recently, experimental studies have shown that CSL boundaries of high CSL density/low Σ value do not crack during fatigue of Ni [17], stress corrosion of a Ni-based superalloy [18], and cavitation of Cu [19].

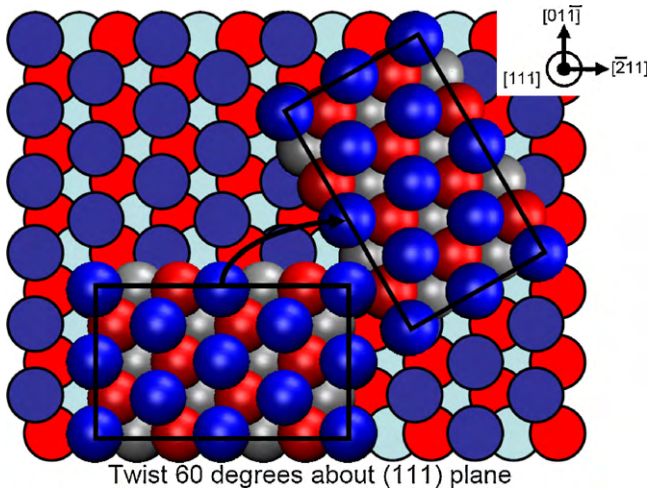

Fig. 3. Schematic of a 60° twist about the ⟨1 1 1⟩ axis representing a (twin) Σ3 GB. By looking at each lattice relative to the supercell background, we can see that the (bottom left) lattice is in perfect agreement but after undergoing the rotation (top right), the blue atoms correspond to the background meanwhile the red and silver atoms are interchanged. (For interpretation of the reference to color in this figure legend, the reader is referred to the web version of the article.)

This is partly attributed to the low Σ value GBs containing a lower distribution of fatigue detrimental intergranular oxides [20]. GBs with an angle less than 15° are referred to as low angle grain boundaries or Σ1 GBs. These GBs have been shown to offer less resistance to dislocation motion, less plastic strain incompatibility, and as a result do not exhibit intergranular fatigue cracking [21]. Read and Shockley modeled low angle GBs as a series of dislocations with an associated energy [22]. Li calculated the stress field associated with low angle GBs as a series of full [23] and partial [24] dislocations, and amended this calculation for high angle GBs [25], although

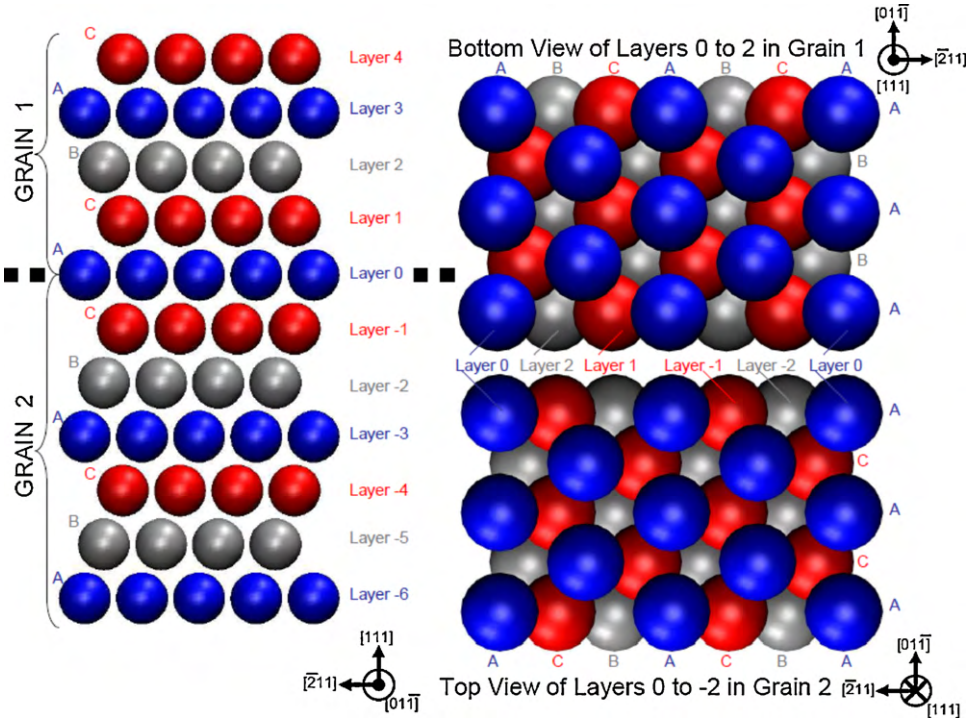

Fig. 2. Schematic of a twin also known as a Σ3 GB, as the grains are tilted 109.47° about the ⟨1 1 0⟩ axis. The dashed line, layer 0, (left) represents the GB and the stacking sequence is mirrored about this plane. By looking along the (1 1 1) plane, we see grain 1 (top right) and grain 2 (bottom right) have the same stacking sequence, although the location of the red and silver atoms are misplaced. Hence, one out of every three atoms are in coincidence from one grain to the next, thus denoting the Σ3 GB in the coincidental site lattice (CSL). (For interpretation of the reference to color in this figure legend, the reader is referred to the web version of the article.)

a significant achievement, the latter model could not capture the complexities of the CSL.

For high angle GBs, Brandon created a criterion, which allowed each GB to have a discrete deviation from a special Σ GB that is proportional to $\Sigma^{-1/2}$ [26]. This has been experimentally confirmed as intergranular fatigue cracking was non-existent for GBs within 3° of a Σ3 coherent twin; the ratio of failure by this mechanism increased for deviations from 3° to 5° and dominated for GBs with deviations greater than 9° [27]. Modifications to the Brandon condition have been proposed by Palumbo and Aust [28], as they modified the exponent, −5/6, to impose a more restrictive upper bound deviation from a CSL and Frary and Schuh [29], whose deviation limit rule requires the angular deviation of one boundary at a triple junction is at most equal to the sum of the other two deviation angles. However, the Brandon condition is still the most widely accepted expression to calculate deviations from a CSL Σ value, and is utilized to characterize what GB can still be denoted as a 'special' boundary.

To leverage the desirable properties of these special CSL GBs, the field of grain boundary engineering emerged. Watanabe was the first to coin the idea of engineering GBs specifically to increase the strength and ductility properties of polycrystals [30] and to control intergranular fracture [31]. Aust et al. expounded the idea of GB engineering to include geometric, energetic, and crystallographic constraints to show that a microstructure composed entirely of low Σ GBs is attainable [32]. External or hydrostatic pressure on the GBs has a significant impact on the GB character, and Shvindlerman and Gottstein addressed this issue as it effects GB free volume, segregation, and junction drag [33].

As the importance of the CSL became more widely recognized, the mathematics of GBs were developed to handle their configuration [34–41]. In 1964, Brandon et al. developed the CSL theory to relate two grains by particular misorientations about specific axes and tabulated these relationships [34]. This inspection method was generalized [35], which enabled 22 CSL values to be categorized up to Σ31 [36]. CSLs were later calculated using matrix theory, which is readily adaptable to computer calculations [37]. One of the most influential CSL papers were produced by Grimmer at al. in 1974 [38], which explained how to obtain a Σ value from a pair of lattices from the rotation matrix, $\Delta\boldsymbol{g}$. The CSL Σ value is found as the least common denominator for each scalar value in $\Delta\boldsymbol{g}$, which they used to tabulate up to Σ49. Since the rotation, $\Delta\boldsymbol{g}$, is not unique, Grimmer described a definition of the disorientation (similar meaning to what we refer to as misorientation) [39], whereas (1) all the components in the tensor $\Delta\boldsymbol{g}$ must be rational values and (2) there must exist a least common multiple, Σ, that makes $\Sigma\cdot\Delta\boldsymbol{g}$ and $\Sigma\cdot\det(\Delta\boldsymbol{g})\cdot\Delta\boldsymbol{g}^{-1}$ integral matrices [40]. This theory was generalized to generate a function for determining CSL Σ values [41]. The mathematics necessary to distinguish CSL GBs from these studies are used extensively in this investigation.

A further level of understanding GBs is obtained by identifying the dislocation arrangement that composes the GB. Sutton and Vitek showed that the atomistic view of the GB can be constructed as a linear combination of dislocations known as the structural unit model (SUM) [42–45]. Each structural unit is associated with a preferred boundary for a given misorientation axis. From this relationship, they deduced that there is a link between the dislocation arrangement at the GB, series of structural units, and GB energy [46,47]. This model has not been widely adopted due to the difficulty in determining the structural units for a given GB, especially for GBs that contain mixed character (3D), high misorientations, or disorientated structures.

The CSL field is tremendously aided by electron back scattering diffraction (EBSD) techniques, which allows an investigator to determine the orientation of each grain in an aggregate. There has been a great deal of work developing EBSD techniques and applying them to CSL configurations, including standard practices [48,49]. The most influential study on the usefulness of CSL structures in polycrystals has been performed by Randle, in which she found that the Σ value of the CSL is a necessary but not sufficient criterion for 'special' properties [50], since each Σ value does not correspond to a unique type of GB. Hence it is necessary to analyze the GB plane and choose an appropriate criterion for deviations from this reference plane [51]. Randle also populated the statistics of various types of boundaries in polycrystals. From this analysis, she found that annealed copper and nickel are composed mostly of tilt GBs rotated about the ⟨1 1 0⟩ axis [50]. If the interface plane in each grain is the same, the tilt boundary is symmetric, if not it is asymmetric. In annealed nickel, 21% of the GBs corresponded to $5 \leq \Sigma \leq 33$, while 46% of the GBs by number fraction were Σ3 types [52], although the latter percentage is higher according to length fraction, i.e. the ratio of the Σ3 boundary length to the total length of the GBs within the 2D EBSD scan [53]. As discussed, there are different types of Σ3 GBs, and it has been shown that after extensive heat treatment, the entire population of the Σ3 GBs is close to the lowest energy configuration in FCC materials, due to reorientation of the GB plane [54]. It has also been observed that GBs dissociate into $\Sigma 3^n$ (Σ1, 3, 9, 81, 243) type to introduce lower energy segments of boundaries [50,51]. These observations about the boundary plane as well as the statistics of GBs within a polycrystal are imperative to our characterization and understanding of GBs.

To fully characterize a grain boundary, one needs to resolve information across five degrees of freedom (DOF) – three to characterize the three unique rotations from one lattice to the next and two more to distinguish the plane separating the two grains. Standard EBSD techniques are two dimensional scans. Hence, to adequately characterize the GB, Rohrer et al. performed an EBSD scan and then serial sectioned a specimen by removing 7 μm via polishing and repeated this process [55]. This procedure collected a 5 DOF GB description through reconstruction of the serial scans, although it is extremely labor intensive. This facilitated a new method to collect the same data based on the probability of line traces [56]. This stereological procedure analyzed the intersection between GB and the specimen surface plane. From the line trace, cubic symmetry properties, grain orientation, and lattice misorientation, a probability is determined for the additional DOFs (i.e. the GB plane). The results of the GB character from this method were similar to the serial sectioning data. This method views peaks within the stereological circle corresponding to the dominant GB planes within the aggregate, but does not resolve the exact plane for a specific GB. From this 5 DOF analysis of GBs in Al and ceramics of low Σ type, the GB plane is most frequently oriented in a low index plane with low surface energy [57]. Further, they observed individual segments containing larger boundary areas had lower relative GB energies in Ni [58]. Using a more deterministic and less laborious method, Ghosh et al. implemented an automated focused-ion beam (FIB) technique to serial section the test specimen inside the same SEM apparatus as the EBSD. This allowed a full 3D computer based reconstruction of the microstructure by aligning and interpolating between the triple points within the microstructure [59,60].

To investigate the grain boundary at a smaller length scale, many researchers have employed atomic simulations. The CSL configuration is well-suited for this investigation, since it is periodic and can be fully described mathematically and, as a result, easily computationally implemented. In a series of papers, Wolf investigated the [1 0 0], [1 1 1], [1 1 0], [1 1 3], and [1 1 2] tilt and twist GBs as well as asymmetric twist GBs [61–64]. From this work, Rittner and Seidman clearly described a technique for generating the GB energies for symmetrical tilts along the [1 1 0] axis and associated this energy with the atomic structure of the GBs and the resulting dislocations arrangement [65]. The most thorough atomistic analysis of GBs to date was performed by Olmsted et al., which created a database for

Table 1
Statistics from the CSL analysis throughout various stages of processing and deformation.

	Billet	Forging	Fatigue-low, $\Delta\varepsilon$	Fatigue-high, $\Delta\varepsilon$	Tensile-20 °C	Tensile-538 °C	Compression low res	Compression high res
Number of grains scanned	4265	7424	3664	2373	3486	3457	3662	704
Total area of grains scanned	9948	37,310	60,542	60,254	56,803	57,198	9963	2479
Average grain size (μm^2)	2.3	5.0	16.5	25.4	16.3	16.6	2.7	3.5
Number of interfaces detected	28,623	47,370	24,018	15,546	21,147	21,118	24,703	4345
GBs within CSL (#)	6593	11,504	6220	3637	5480	5329	6524	1275
GBs within CSL (in %)	23.03	24.29	25.90	23.40	25.91	25.23	26.41	29.34
LAGBs – $\Sigma 1$ (#)	1841	1718	1083	480	2588	2278	1157	156
LAGBs – $\Sigma 1$ (in %)	6.43	3.63	4.51	3.09	12.24	10.79	4.68	3.59
Twins – $\Sigma 3$ (#)	2401	5330	2915	1758	1320	1455	3467	735
Twins – $\Sigma 3$ (in %)	8.39	11.25	12.14	11.31	6.24	6.89	14.03	16.92

the energies and mobilities of symmetrical and asymmetrical (388 total) boundaries in Ni and Al [66,67]. Out of all the GBs surveyed, the coherent twin (of type $\Sigma 3$) had the lowest energy and mobility. Many of the procedures used in these studies aid the current work.

It has been established that both the grain size and grain boundary character play an important role in the mechanical behavior of the material. Although in the literature, these two microstructural aspects have been treated separately. In this study, we correlate the role of GB character, specifically GB energy to the grain size. Further, we analyze the GB character for a range of material processes and deformations from billet to forging to experiments (tensile, compression, and fatigue), in order to characterize the evolution of the GB and as a consequence its effect on mechanical behavior.

2. Experimental

The material utilized in this study is a Ni-based superalloy, Udimet 720 (U720). The primary strengthening mechanism in this material is in the form of ordered Ni_3Al precipitates ($L1_2$ structure), which occurs in this material at three length scales (primary, secondary, and tertiary). The coherency of these γ' precipitate with respect to the γ matrix offers stability along with enhanced strengthening at elevated temperatures. The material underwent a solution process at 1100 °C for 2 h followed by oil quenching, in order to prepare the matrix for uniform precipitation of γ'. Afterwards, it was aged at 760 °C for 8 h with air-cooling, in order to precipitate the coarser γ', which offers creep resistance. A second aging process at 650 °C for 24 h with air-cooling produced fine γ' for strengthening the microstructure for tensile and fatigue loads and stabilizing the γ' precipitates.

Also, during the heat treatment process the γ' acts to pin the grain boundaries, thus determining the grain size in the γ matrix. In this material, there are areas of densely populated γ' along side areas denuded of γ', as shown in Fig. 4a. As a result, a wide distribution of grain sizes exists, as fine grains form in regions of heavily populated γ' and coarse grains form in regions where γ' is sparse.

Data on grain size and orientation were obtained from EBSD scans. Prior to EBSD, the samples were electropolished utilizing a solution composed of 60 vol.% methanol, 34 vol.% butanol, and 6 vol.% perchloric acid at −20 °C. The raw data obtained were first analyzed using HKL commercial software from TSL [68] to obtain grain orientations. The mean grain area is 4 μm^2 although grains can reach over 100 μm^2 (Fig. 4b). Thus, a small step size in the EBSD scans had to be used to accurately cover the small grains. At the same time, the bigger grains required large area scans for statistically meaningful data. Thus, in a typical scan, a few thousand grains were analyzed, as shown in Table 1. However, the good signal to noise ratio of the EBSD patterns obtained from the electropolished samples, allowed for relatively fast data acquisition for a single pattern, resulting in acceptable total measurements times. The long tail of the grain size distribution and dual peaks shown in Fig. 4b suggests a bi-modal like distribution of grain sizes with large variations. Further, due to the variation in grain sizes and neighboring grains, each grain can have a wide distribution of associated GBs. Given a sufficiently large sample size, a 2D EBSD measurement of the grain area is capable of producing accurate representation of the grain size compared to 3D data [69]. A histogram of the number of GBs belonging to each grain is shown in Fig. 4c. A typical 2D scan showed that each grain has a mean value of 5 interfaces, but some grains had as many as 20 GBs.

In this study, seven U720 samples were investigated: 2 fatigue specimens (tested at 1.3% and 0.9% strain ranges at 538 °C), 2 tensile tests (538 °C and room temperature, which failed with a ductility of ~20%), billet material, a specimen from the forging in the as-received condition, and a specimen compressed to an engineering strain of ~16%. From the EBSD scans of these 7 specimens, a total of 29,035 grains were analyzed.

3. Results

3.1. CSL procedure

The EBSD results showed that the billet, forged, and fatigue specimens were not textured, i.e. the orientations of the grains within the aggregate displayed nearly a random distribution. Therefore, the fatigue loading of the specimens did not result in grain rotation or texturing of the material at low and high strain ranges. Meanwhile, the monotonic tensile and compression specimens displayed a ⟨1 1 1⟩ and ⟨1 1 0⟩ texture, respectively. As expected, due to the large deformations each specimen experienced during testing, the grains in the polycrystalline material rotated and aligned to the loading axis. For each case, the primary slip caused the tensile and compression axes to rotate towards the [1 0 1] and [1 1 $\bar{1}$] slip directions, respectively.

From the EBSD scan, the orientation of each grain (Euler angles) in the scan and a list of the neighboring grains was obtained. From the Euler angles (φ_1, Φ, φ_2), the rotation matrix, $\mathbf{g}$, of each grain is then found by:

$$\mathbf{g} = \begin{bmatrix} \cos\varphi_1\cos\varphi_2 - \sin\varphi_1\sin\varphi_2\cos\Phi & \sin\varphi_1\cos\varphi_2 + \cos\varphi_1\sin\varphi_2\cos\Phi & \sin\varphi_2\sin\Phi \\ -\cos\varphi_1\sin\varphi_2 - \sin\varphi_1\cos\varphi_2\cos\Phi & -\sin\varphi_1\sin\varphi_2 + \cos\varphi_1\cos\varphi_2\cos\Phi & \cos\varphi_2\sin\Phi \\ \sin\varphi_1\sin\Phi & -\cos\varphi_1\sin\Phi & \cos\Phi \end{bmatrix}. \quad (1)$$

This allows us to calculate the misorientation rotation matrix, $\Delta\mathbf{g}$, between each grain and its neighbor,

$$\Delta\mathbf{g} = \mathbf{g}_1^{-1}\mathbf{g}_2. \quad (2)$$

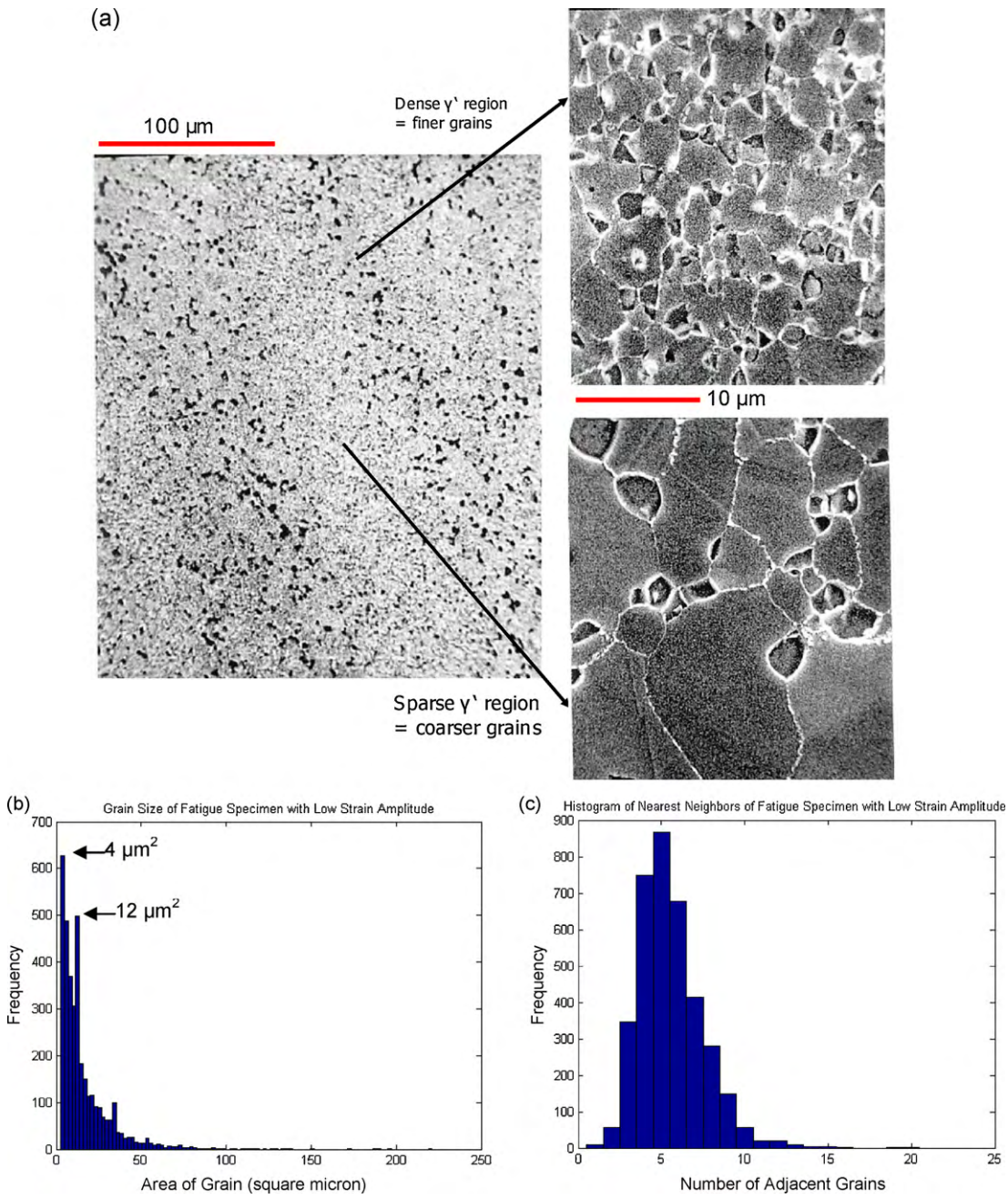

Fig. 4. (a) Microstructure of U720, displaying bands of γ′ precipitates (left). These precipitates determine the grain size. In areas of densely populated γ′, the grain size is fine, while in areas denuded of γ′, the grain size is coarse. The scale bars are shown in red. (b) Histogram of the grain area. (c) Histogram of the number of nearest neighbors from a 2D EBSD scan. (For interpretation of the reference to color in this figure legend, the reader is referred to the web version of the article.)

However, the misorientation matrix is not unique, since FCC materials have cubic symmetry. Thus, the misorientation matrix must be rotated about threefold axes (plus the identity) or in other words multiplied by the 24 cubic symmetry operators (known as class 432, $\boldsymbol{O_{432}}$), where each symmetry operator is a rotation of the identity tensor. A loop is created over each symmetry operator to ensure that a minimum value of the misorientation between grains, Θ, is found.

$$\Theta = \min \left| \cos^{-1} \left\{ \frac{tr(\boldsymbol{O}_{432} \Delta \boldsymbol{g}) - 1}{2} \right\} \right| \tag{3}$$

During the EBSD scan, the minimum misorientation to define a GB was specified as 2°, hence between two points a misorientation less than 2° was categorized as an internal grain rotation, whereas a larger misorientation indicated the presence of a GB.

As described earlier, we need a total of five degrees of freedom to fully characterize a GB, three for the misorientation and two to describe the plane of the GB [48–60,66,67]. In this work, we utilize an axis–angle pair scheme, which specifies the misorientation across the GB with an axis of misorientation (UVW) along with an angle (θ), as shown in Fig. 5.

$$\theta = \cos^{-1} \left(\frac{\Delta \boldsymbol{g}_{11} + \Delta \boldsymbol{g}_{22} + \Delta \boldsymbol{g}_{33} - 1}{2} \right) \tag{4}$$

$$(U, V, W) = \frac{(\Delta \boldsymbol{g}_{23} - \Delta \boldsymbol{g}_{32}, \Delta \boldsymbol{g}_{31} - \Delta \boldsymbol{g}_{13}, \Delta \boldsymbol{g}_{12} - \Delta \boldsymbol{g}_{21})}{\sqrt{(\Delta \boldsymbol{g}_{23} - \Delta \boldsymbol{g}_{32})^2 + (\Delta \boldsymbol{g}_{31} - \Delta \boldsymbol{g}_{13})^2 + (\Delta \boldsymbol{g}_{12} - \Delta \boldsymbol{g}_{21})^2}} \tag{5}$$

This gives the GB misorientation but not the GB plane. Thus, the description of the GB is matched with the axis–angle pair to specify its CSL value according to a reference table provided by Grimmer et

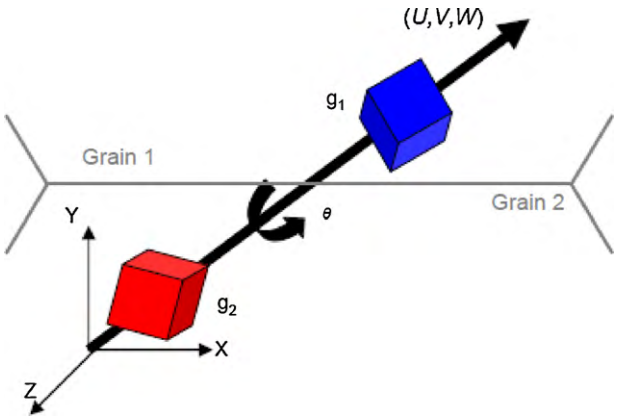

Fig. 5. Schematic of the axis–angle pair for grain boundary description.

al. that includes the axis–angle pair for 47 Σ values from Σ3 to Σ49 [38]. The allowable tolerance between the measured and reference value of axis and angle is given using the Brandon condition [26]:

$$\vartheta = \vartheta_o \Sigma^{-1/2}, \quad (6)$$

where ϑ_o is the misorientation limit for a low angle GB, set at 15°. Thus, a low angle GB is defined as a misorientation in the range of 2°–15° and denotes a Σ1 GB. The Brandon condition has been chosen in this investigation compared to other criteria due to its accuracy and widespread application in the literature. Hence, from this description, a Σ3 GB can have a deviation up to 8.66° and still display 'special' properties, which has been confirmed by experiments [27]. Further, the Brandon condition is invoked on each component of the axis–angle pair, thus $\left|\theta' - \hat{\theta}\right| \leq \vartheta$ and $\left|(U', V', W') \cdot (\hat{U}, \hat{V}, \hat{W})\right| \leq \vartheta$ must be satisfied to define a Σ GB, where the â and ′ denotes the reference and measured values, respectively.

It should be noted that the CSL Σ value is not a unique description of the GB, although for ease of reporting, we plot the CSL Σ values, as shown in Figs. 6–10, albeit all calculations are performed based on the axis–angle pair description of the GB. In Fig. 6, a histogram is shown of the CSL values for U720 material from the billet and forging. It can be seen that approximately 60% of the CSL values are comprised of low angle GBs (Σ1s) and twins (Σ3s). The amount of low angle GBs decrease during the forging process as the large deformation leads to additional misorientation within the aggregate of grains. The forging material has undergone a heat treatment, which increases the population of annealing twins

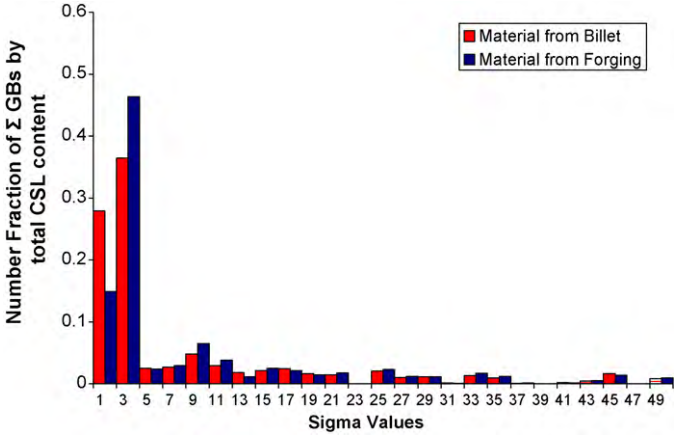

Fig. 6. Histogram of CSL values for material from billet and forgings of U720.

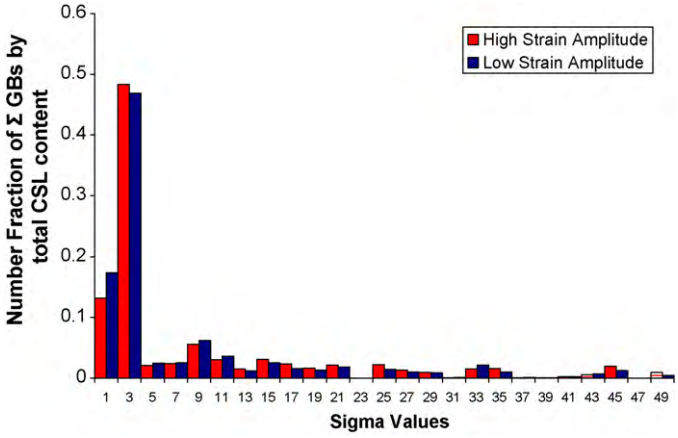

Fig. 7. Histogram of CSL values for specimens of U720 after fatigue testing at 538 °C.

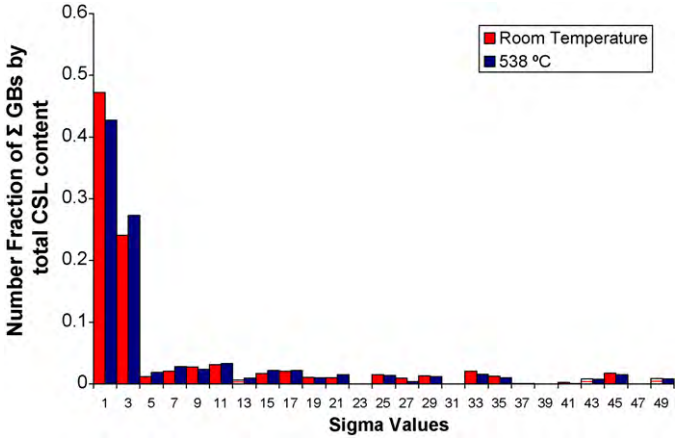

Fig. 8. Histogram of CSL values for specimens of U720 after tensile testing to failure (approximate ductility of ~20%).

within the material and as a consequence the population of Σ3 GBs.

Similarly, the CSL values were measured from EBSD scans of fatigue specimens after failure, as shown in Fig. 7. Interestingly, the CSL Σ values and GB character distributions did not substantially change from forging to fatigue testing regardless of the applied strain amplitude. Hence, during fatigue deformation, the

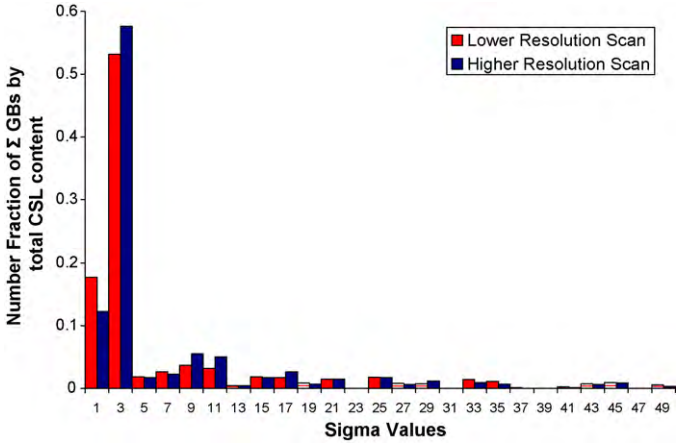

Fig. 9. Histogram of CSL values for specimens of U720 after compression testing to approximately 16% engineering strain obtained through our EBSD analysis at two different scanning resolutions.

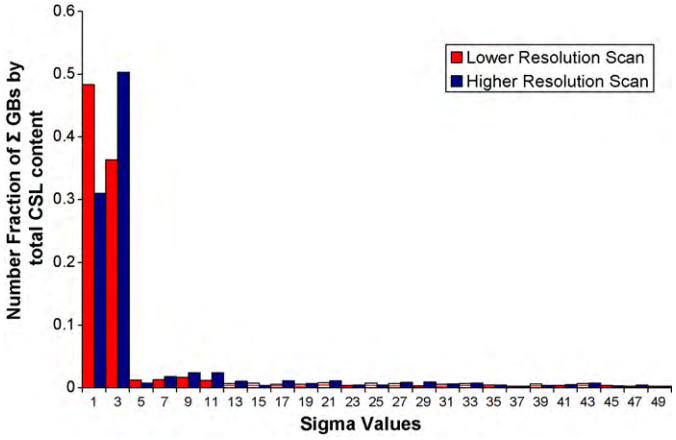

Fig. 10. Histogram of CSL values for specimens of U720 after compression testing to approximately 16% engineering strain obtained through EBSD analysis at two different scanning resolutions. Analysis is completed with commercial HKL software by looking at pixilated segments along the GB.

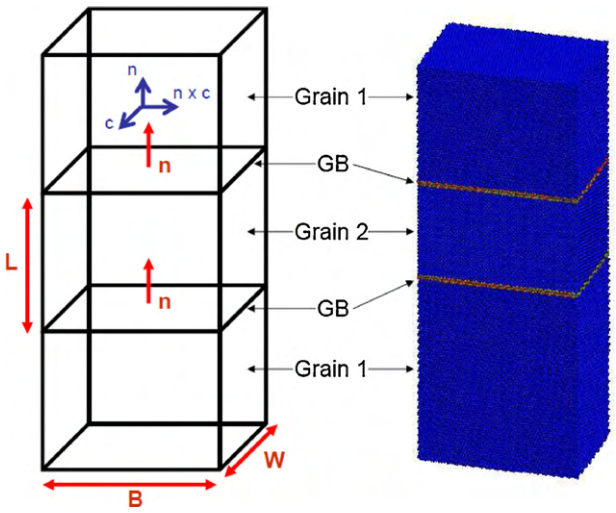

Fig. 11. Grain boundary set-up for the atomic simulation displaying a pair of GBs per system. The normal to the GB, ***n***, represents the boundary plane. The axis of rotation for tilt and twist GBS is ***c*** and ***n***, respectively. The geometry (*L*, *B*, *W*) is chosen to satisfy periodic boundary conditions and avoid GB–GB interactions.

Σ GBs stayed intact. By contrast, tensile testing resulted in more unidirectional deformation to the specimen and a change in CSL distribution, as shown in Fig. 8. The tensile specimens failed at a ductility of approximately 20%, and, as previously mentioned, the primary slip rotated the tensile axis to the [1 0 1] direction resulting in ⟨1 1 1⟩ texture. In doing so, the GB characters were redistributed into mostly Σ1 low angle GBs, thus annihilating many of the Σ3 twins. The difference in test temperature from 20 °C to 538 °C did not have a significant impact in the CSL distribution.

Fig. 9 shows CSL data obtained with EBSD on a compression specimen tested to approximately 16% engineering strain. As previously discussed, the large amounts of strain forced the compression axes to rotate towards the [1 1 $\bar{1}$] slip direction resulting in ⟨1 1 0⟩ texture, although the CSL distribution did not dramatically change as was the case under tensile loading. There existed a slight increase in low angle GBs due to the increase in texture and alignment of grains. Also, the population of Σ3 GBs slightly increased, which could possibly be attributed to deviations within the microstructure as a smaller sample area was scanned. The EBSD measurements on this compression specimen were performed at two distinct resolutions, in order to check the statistical significance of the data. The results were not substantially different; although due to the increase in magnification, fewer grains with a different number of data points per grain were scanned in the high magnification case. This is not surprising as the procedure that was described above analyzed the orientation over an entire grain and defined the GB relative to the orientation of each neighboring grain. The CSL results for each specimen analyzed using our method are summarized in Table 1, which gives the values for the number of grains and grain boundaries detected during the EBSD scan. Further the quantified values are reported for the average grain size, ratio of CSL boundary content versus the total number of GBs (including irrational types), and population of low angle grain boundaries and twins.

As discussed, our method views the average orientation of each grain via its Euler angles and compares the information to its neighboring grains. Thus the information received about the CSL corresponds to the entire GB segment between adjacent grains. This methodology is in stark contrast to commercial codes such as HKL [68]. In such software, the EBSD analysis is performed in a point by point grid. Any misorientation between two points greater than a threshold (2° by default) is designated as a GB. Hence, the GB is composed of pixilated and serrated fragments. As a consequence, the reported CSL values are also pixilated; thus a segment between two adjacent lattices can be comprised of fragments containing various CSL characters. In this case, the resolution of the EBSD scan plays an important role in determining the CSL distribution as shown in Fig. 10, as the histogram is considerably changed for a high versus low resolution scan across the same material.

Further, the CSL characters of the entire GB segment separating adjacent grains are physically more relevant versus a pixilated view. Hence, the CSL distributions obtained from the two methods are essentially different techniques and do not yield the same type of information as shown comparing Figs. 9 and 10. Although we contend that the information presented in Fig. 9 from our methodology is more pertinent to the mechanical behavior and physics of the grain boundary as is the aim of this investigation. The next level of understanding the role of GBs is to measure their energy values through atomic simulations as described in the next section.

3.2. GB energy

To capture the physics at the grain boundary interface, it is necessary to investigate this problem at a smaller scale. Atomic simulations were utilized in the form of a molecular dynamics (MD) code called LAMMPs [70,71] to study the effects of grain boundary misorientation on the energy of its interface and to service our model. A system was set up to investigate a grain with a specific (mis)orientation 'sandwiched' between two similar grains, representing a specific tilt or twist GB with a corresponding CSL Σ value, as shown in Fig. 11. Grains 1 and 2 in the structure were created with a specific orientation to represent distinct CSL boundaries (Table 2), in which the boundary plane is represented by ***n***. For tilt and twist GBs, the axis of rotation is represented by ***c*** and ***n***, respectively.

In each structure, the FCC lattice is comprised of atoms with the Foiles–Hoyt Ni embedded atom method (EAM) potential, chosen to match the stable and unstable stacking fault energy of the material [72]. This EAM potential for Ni was chosen to match the intrinsic, γ_{SF}-127 mJ/m^2, and unstable, γ_{US}-255 mJ/m^2, stacking fault energies of the material, which compares well with experimental values of 125–128 mJ/m^2 and ab initio calculations of 273 mJ/m^2 for the γ_{SF} and γ_{US} energies, respectively [73]. Also, the lattice constant of this EAM potential, 3.52 Å, exactly matches that of nickel. Periodic boundary conditions are enforced in all three directions to represent bulk material, and the simulation cell is of sufficient size (*L*, *B*, *W* refer to Fig. 11) to negate boundary–boundary strain field

Table 2
For each tilt and twist GB, the axis and angle of rotation is displayed along with the resulting CSL Σ value and boundary plane normal. For tilt GBs, the axis of rotation is normal to the boundary plane. For twist GBs, the axis of rotation aligns with the boundary plane normal.

⟨1 1 0⟩ Tilt GBs				⟨1 1 1⟩ Twist GBs				⟨0 0 1⟩ Tilt GBs			
Rotation axis	Rotation angle (°)	Σ value	Boundary plane	Rotation axis	Rotation angle (°)	Σ value	Boundary plane	Rotation axis	Rotation angle (°)	Σ value	Boundary plane
[1 1 0]	0.00	1	{0 0 1}	[1 1 1]	0.0	1	{1 1 1}	[0 0 1]	0.0	1	{1 0 0}
[1 1 0]	13.44	73	{1,1,12}	[1 1 1]	9.4	111	{1 1 1}	[0 0 1]	14.3	65	{8 1 0}
[1 1 0]	20.05	33	{1 1 8}	[1 1 1]	13.2	57	{1 1 1}	[0 0 1]	16.3	25	{7 1 0}
[1 1 0]	26.53	19	{1 1 6}	[1 1 1]	17.9	31	{1 1 1}	[0 0 1]	22.6	13	{5 1 0}
[1 1 0]	31.59	27	{1 1 5}	[1 1 1]	21.8	21	{1 1 1}	[0 0 1]	26.0	89	{13,3,0}
[1 1 0]	38.94	9	{1 1 4}	[1 1 1]	26.0	237	{1 1 1}	[0 0 1]	28.1	17	{4 1 0}
[1 1 0]	44.00	57	{2 2 7}	[1 1 1]	27.8	13	{1 1 1}	[0 0 1]	36.9	5	{3 1 0}
[1 1 0]	50.48	11	{1 1 3}	[1 1 1]	32.2	39	{1 1 1}	[0 0 1]	41.1	73	{8 3 0}
[1 1 0]	58.99	33	{2 2 5}	[1 1 1]	38.2	7	{1 1 1}	[0 0 1]	48.9	73	{11,5,0}
[1 1 0]	70.53	3	{1 1 2}	[1 1 1]	42.1	93	{1 1 1}	[0 0 1]	53.1	5	{2 1 0}
[1 1 0]	80.63	43	{3 3 5}	[1 1 1]	44.8	129	{1 1 1}	[0 0 1]	61.9	17	{5 3 0}
[1 1 0]	86.63	17	{2 2 3}	[1 1 1]	46.8	19	{1 1 1}	[0 0 1]	64.0	89	{8 5 0}
[1 1 0]	93.37	17	{3 3 4}	[1 1 1]	49.6	5	{1 1 1}	[0 0 1]	67.4	13	{3 2 0}
[1 1 0]	99.37	43	{5 5 6}	[1 1 1]	52.7	61	{1 1 1}	[0 0 1]	73.7	25	{4 3 0}
[1 1 0]	109.47	3	{1 1 1}	[1 1 1]	60.0	3	{1 1 1}	[0 0 1]	75.7	65	{9 7 0}
[1 1 0]	121.01	33	{5 5 4}					[0 0 1]	77.3	41	{5 4 0}
[1 1 0]	129.52	11	{3 3 2}					[0 0 1]	79.6	61	{6 5 0}
[1 1 0]	141.06	9	{2 2 1}					[0 0 1]	90.0	1	{0 1 0}
[1 1 0]	148.41	27	{5 5 2}								
[1 1 0]	153.47	19	{3 3 1}								
[1 1 0]	159.95	3	{4 4 1}								
[1 1 0]	166.56	73	{6 6 1}								
[1 1 0]	180.00	1	{0 0 1}								

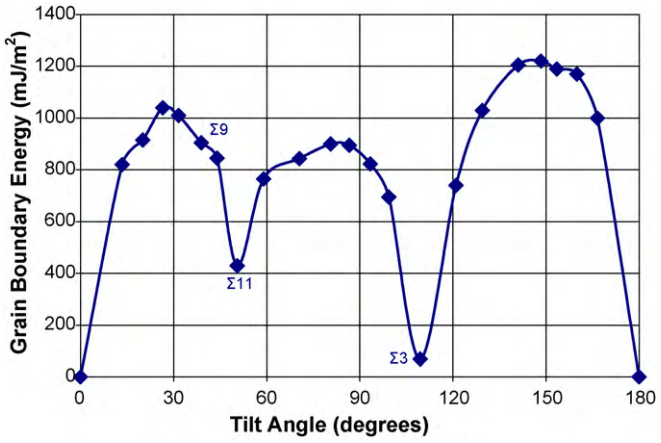

Fig. 12. The grain boundary energy shown as a function of the tilt angle for nickel in the ⟨1 1 0⟩ direction.

interactions or 'cross-talk' of the GBs:

$$L = \alpha\sqrt{h^2 + k^2 + l^2} \geq 8\,\text{nm} \tag{7}$$

$$B, W = \beta\sqrt{h^2 + k^2 + l^2} \geq 5\,\text{nm} \tag{8}$$

where h, k, l are the Miller indices for the three orthogonal vector representations of each grain orientation and α and β are scalars to satisfy the size requirements.

The system is first annealed to 800 K and then quenched to 10 K, afterwards the atoms are statically equilibrated or 'relaxed' using the conjugant gradient method to obtain the energy of the system of N atoms containing the pair of CSL boundaries, $E_{\text{CSL}}^{\text{GB}}$. Further, the box dimension in only the direction normal to the GB was allowed to relax in order to alleviate any GB pressure. The energy associated with the grain boundary was calculated by the following:

$$\gamma_{\text{GB}} = \frac{E_{\text{CSL}}^{\text{GB}} - (N/M)\cdot E_{\text{Perfect}}^{\text{FCC}}}{2A}, \tag{9}$$

where A is the area of the GB ($B{\cdot}W$) and the factor of two is necessary since the system contains two GBs. In order to isolate the GB energy, we must remove the potential energy of the atoms in the lattice, $E_{\text{Perfect}}^{\text{FCC}}$ (4.45 eV per M atoms).

The simulation was repeated for various twist and tilt grain boundary angles about various axes as the set-up details are listed in Table 2 and the results are shown in Figs. 12–14. In Fig. 12, a tilt GB is constructed about a rotation along the ⟨1 1 0⟩ axis of the crystal. It can be seen that this curve contains local minimums and

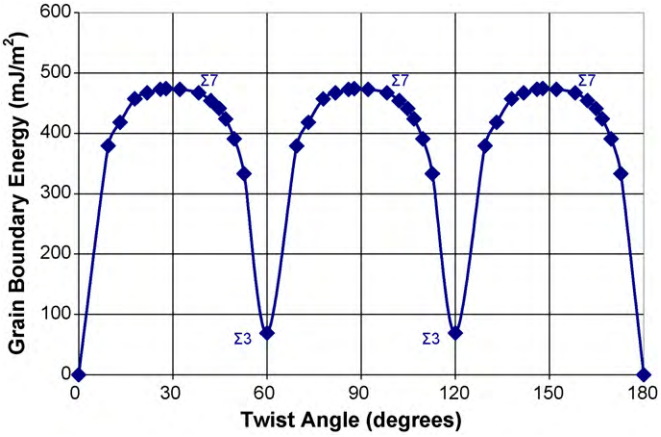

Fig. 13. The grain boundary energy shown as a function of the twist angle for nickel in the ⟨1 1 1⟩ direction.

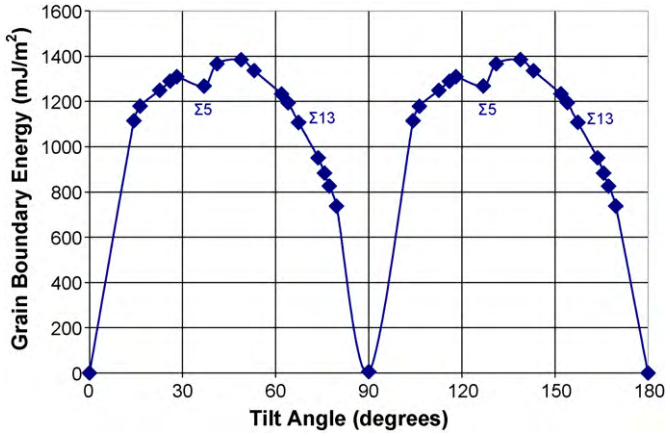

Fig. 14. The grain boundary energy shown as a function of the tilt angle for nickel in the ⟨0 0 1⟩ direction.

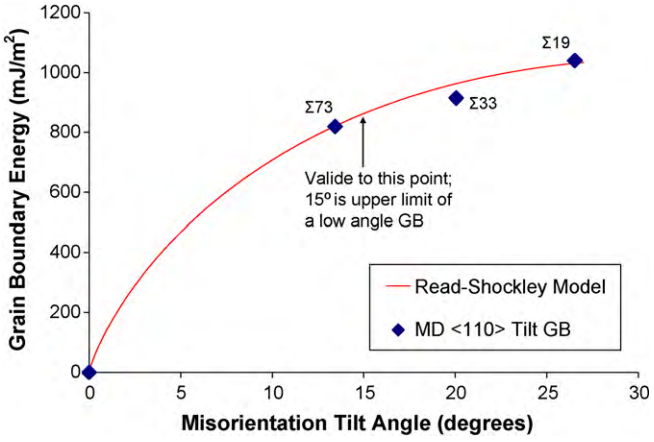

Fig. 15. Comparison of GB energies from the Read–Shockley model (a continuum description of low angle grain boundaries valid for misorientations from 2° to 15°) and calculations from MD results of CSL values in and around that range.

cusps corresponding to preferred energy configurations as a result of the special Σ GBs in the CSL, which concurs with simplified defect structures at the interface as described by the structural unit model [42–47,65]. At a rotation of 0°, the atoms are in a perfect lattice configuration. At a rotation of 50.48°, the defect structure at the interface is simple, therefore corresponding to a local minimum in the energy and the Σ11 GB. A 109.47° tilt rotation about the ⟨1 1 0⟩ axis has the lowest energy of any GB, which corresponds to a very simple defect structure known as a coherent twin or the Σ3 GB, as previously shown in Fig. 2. For this reason, these boundaries are most abundant in this material as annealing twins form during processing, as shown in Figs. 6 and 7. A characterization of 900 GBs in pure annealed nickel performed by Randle showed that over half of the interfaces consist of ⟨1 1 0⟩ tilt GBs [50]. Hence, the ⟨1 1 0⟩ tilt GBs are a preferred interface configuration and of importance for FCC materials and nickel alloys.

Other types of GBs, specifically ⟨1 1 1⟩ twist and ⟨0 0 1⟩ tilt, were analyzed as shown in Figs. 13 and 14, respectively. Each plot was mirrored about a line of symmetry corresponding to the boundary plane on the FCC lattice, which is 90° for each case. The minimum points in Fig. 13 correspond to a 60° twist rotation about the ⟨1 1 1⟩ axis and a coherent twin (Σ3 GB), which is shown in Fig. 3. Hence, we see that the same GB is characterized by a 109.47° tilt about the ⟨1 1 0⟩ axis and a 60° twist about the ⟨1 1 1⟩ axis. The local cusps in Fig. 14 correspond to the Σ5 GB.

The energies of the large angle GBs are calculated through atomic simulations. The CSL configuration is well-suited for this investigation, since it can be fully described mathematically, is periodic, and, as a result, easily computationally implemented. However, the low angle GBs cannot be fully characterized by a CSL, since they are not fully periodic. Hence, the energies of these boundaries are calculated by the Read–Shockley model, in which low angle GBs are modeled as a series of dislocations and their resulting energies are calculated through linear elastic isotropic continuum theory [22]:

$$E = E_o\theta(A - \ln\theta), \tag{10}$$

where $E_o = \mu b/4\pi(1-\nu)$ and $A = 1 + \ln(a_o/2\pi r)$.

In the Read–Shockley model, θ is the misorientation between grains in radians, μ is the shear modulus, υ is the Poisson ratio, $\boldsymbol{b}$ is the Burgers vector, a_o is the lattice spacing, and r is the cutoff radius of the dislocation core. This formula is valid for misorientations from 2° to 15° and compares well to the few MD results of CSL values for small misorientations about the ⟨1 1 0⟩ tilt axis, as shown in Fig. 15. Therefore, the energies are calculated from the Read–Shockley model for low angle GBs and measured from MD for high angle GBs. The next step in this analysis is to link these energies to the spatial EBSD scans for this material.

4. Linking characterization to energetics and discussion

As previously discussed, to fully characterize a GB, we need a total of five degrees of freedom [48–60,66,67], although from the 2D EBSD scan and the axis–angle pair analysis, the GB normal is not available. This information can be obtained using serial sectioning of the test specimen [59,60], although this method is a time consuming process in terms of data collection/interpretation and requires extensive equipment/software. In this procedure, we have calculated the axis–angle pair for each grain in the aggregate from an EBSD scan. Further, we have calculated the energies of the GBs via MD simulations and the Read–Shockley model, which we can use the Miller indices (*hkl*) description of the lattice to back-calculate the axis–angle pair. Hence, through the axis–angle pair, we have a direct comparison to correlate the measured GB orientations of U720 from EBSD scans to the GB energy from MD simulations. We employ a simple assumption for the case of duplicate values of the axis–angle pairs, where the GB character is chosen based on the description of the GB containing the lowest energy value. During heat treatment of the material, the GB contains sufficient mobility to reorient itself into a low energy configuration. This assumption has validity as GB normals have been experimentally shown by Randle to reorient to lower energy configurations [50–52,54] and in cases with sufficiently long heat treatments, the GBs are comprised of the lowest energy configurations [51]. Similarly, Rohrer et al. experimentally found that the GB plane is most frequently oriented such as to posses a low index plane with low surface energy [57]. Further, by MD simulations, Olmsted et al. showed that the coherent twin has the lowest GB energy and mobility, meanwhile GBs with higher energy also have higher mobility [66,67]. Hence, GBs with higher energies have a higher mobility and driving force to reorient the GB normal into a lower energy configuration. Consequently, the 5 DOF description of a GB can be replaced by an axis–angle pair, reasonably well, where redundancies converge to the lowest energy configuration of the GB.

The grain boundary character developed through EBSD scans is linked to atomic simulations for high angle grain boundaries to measure properties and behavior of the GB that cannot be obtained through experiments. Table 2 displays each of the 56 GB systems analyzed in this study, which is supplemented by a database with the energies of 388 GBs [66]. For low angle grain boundaries, we

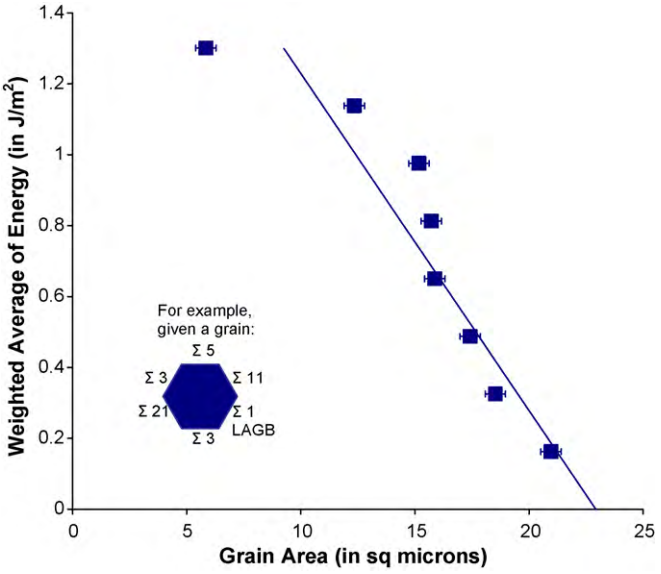

Fig. 16. GB energy versus grain size (area) for a low strain amplitude fatigue specimen of U720 tested at 538 °C. The graph is based on a scan containing 3664 grains. The (normalized) GB energies obtained via MD are summed per grain and normalized by the number of GB segments per grain (refer to insert). These energies are plotted against the GB area, displaying an inverse correlation as shown by the best fit line through the data. For ease of plotting, the energies are binned and the grain areas are averaged.

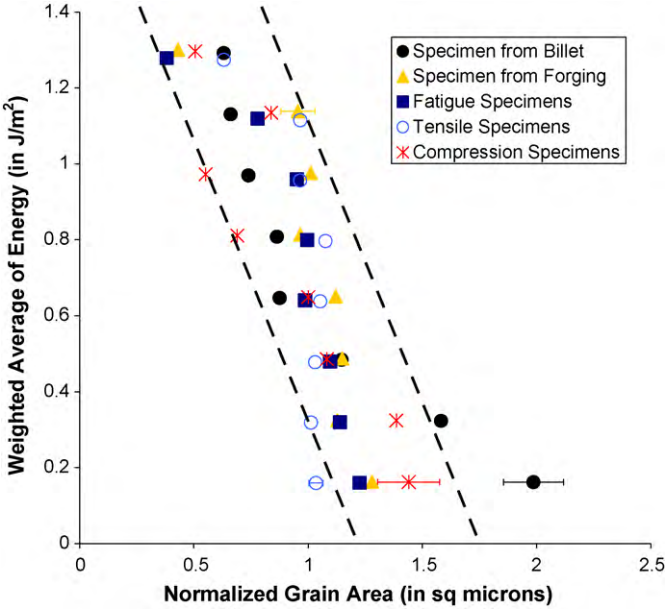

Fig. 17. GB energy versus grain size (area) for 7 specimens: 1 specimen from billet, 1 specimen from forging, 2 fatigue specimens, 2 tensile specimens, and 1 compression specimen. A total of 29,035 grains were analyzed in the EBSD scans across all 7 specimens. The same inverse correlation behavior between GB energy and grain size is shown in each specimen. In this figure, the dashed lines are drawn to guide the eyes.

employ the Read–Shockley model to calculate the energy [22]. Thus, the spatial map of the GB characters and grain size from EBSD scans are linked to the GB static relaxed energy from atomistic simulations. The GB energy is measured as a normalized value (mJ/m^2). Each 2D scan of a grain is composed of multiple GB segments; the energies of each segment are summed and normalized by the number of GB segments as each grain may contain a different number of neighboring grains. The GB energy is seen to be inversely proportional to grain size (in terms of area) as shown for the low strain amplitude fatigue specimen in Fig. 16. This EBSD scan contained 3664 grains. In order to clearly graph this data, the GB energy has been binned and the grain area is averaged within each bin and the standard deviation for the bins is also shown. This procedure has been repeated for each of the 7 test specimens, and the same GB energy-grain area inverse correlation behavior was obtained for each specimen, as shown in Fig. 17.

The results of this analysis show that larger grains exhibit a smaller specific energy. We contend that the reasons are threefold. Twins are more prone to occur in larger grains as evident by a TEM analysis of this material. Thus due to the large amount of annealing twins present in large grains, the overall specific interface energy is lower for larger grains. Also, during heat treatment, larger grains have more mobility, thus they can orient themselves in favorable low energy configurations, while smaller grains are merely pinned. In other words, large grains grow until they reach a low energy configuration. Finally, a small grain exhibits more curvature in the GB, which also contributes to a higher energy. Recently, Rohrer et al. established that an individual segment of a given boundary is prone to have a larger area when the GB character displays a lower energy value in Ni [58]. Our analysis emphasizes this relationship and extends the correlation between length scale and energetics. For the first time, a link is made between the grain size and energies of the sum of its associated grain boundaries for a given grain. Every GB character for a given grain is examined and we establish an inverse relationship between the total interface energy and grain size.

5. Conclusions

This work has outlined considerable progress in characterizing grain boundaries in an engineering alloy and linking this information to grain size through the use of CSL distribution and GB energy. We have utilized a methodology to examine a GB as the entire region separating two grains and link it to a CSL description. The evolution of the CSL has been shown for various stages of processing (billet and forging) and deformation (tension, compression, and fatigue). Fatigue testing has little effect on the CSL distribution, although large deformation processes such as tension and compression lead to rotation and alignment of the grains and a greater population of low angle GBs. In each of the specimens, the $\Sigma 3$ GBs were prevalent, and it was shown that these represent coherent annealing twins.

The energies of the CSL GBs were measured using MD, while the Read–Shockley model was used to calculate low angle GBs. The lowest energy configuration was observed for the coherent $\Sigma 3$ twin GB, which explains its abundance in the measured EBSD analysis. A link was made between the calculated energies and the EBSD measurements of grain orientation and size. A strong inverse correlation exists between grain boundary energy and grain size for each specimen. The rationale behind this stems from larger grains exhibiting a greater twin density, more mobility to reorient the GB normal during heat treatment, and less GB curvature.

Acknowledgments

Materials and support for this work was provided by Rolls-Royce Corporation and partial support was provided by NSF DMR 0803270. The authors would like to acknowledge Professor Duane D. Johnson of the University of Illinois, Urbana-Champaign for his assistance in the atomic simulations, Professor David Olmsted of Northeastern University for supplementing our MD study with his database of grain boundary energies, and Dr. Stephen M. Foiles of Sandia National Laboratory for sharing his nickel EAM potential.

References

[1] J.P. Hirth, Metallurgical Transactions A (Physical Metallurgy and Materials Science) 3 (1972) 3047.
[2] E.O. Hall, Proceedings of the Physical Society B 64 (1951) 747.
[3] N.J. Petch, Iron and Steel 26 (1953) 601.
[4] M.F. Ashby, Philosophical Magazine 21 (1970) 399.
[5] J.C.M. Li, Y.T. Chou, Metallurgical Transactions 1 (1970) 1145.
[6] D.A. Curry, J.F. Knott, Metal Science 10 (1976) 1.
[7] A. Curry, J.F. Knott, Metal Science 12 (1978) 511.
[8] G.M. Sinclair, W.J. Craig, Influence of Grain Size on Work Hardening and Fatigue Characteristics of Alpha Brass, 1952, United States, pp. 18, (Reprint).
[9] A.W. Thompson, Scripta Metallurgica 5 (1971) 859.
[10] A.W. Thompson, W.A. Backofen, Acta Metallurgica 19 (1971) 597.
[11] A.W. Thompson, W.A. Backofen, Metallurgical Materials Transactions A (Physical Metallurgy and Materials Science) 2 (1971) 2004.
[12] P. Lukas, L. Kunz, Materials Science and Engineering 85 (1987) 67.
[13] D.J. Morrison, J.C. Moosbrugger, International Journal of Fatigue 19 (1997) S51.
[14] H.W. Liu, International Journal of Fracture 96 (1999) 331.
[15] S. Berbenni, V. Favier, M. Berveiller, International Journal of Plasticity 23 (2007) 114.
[16] M.L. Kronberg, F.H. Wilson, American Institute of Mining and Metallurgical Engineers – Journal of Metals 1 (1949) 501.
[17] L.C. Lim, Acta Metallurgica 35 (1987) 1653.
[18] Y. Pan, B.L. Adams, T. Olson, N. Panayotou, Acta Materialia 44 (1996) 4685.
[19] D.P. Field, B.L. Adams, Acta Metallurgica et Materialia 40 (1992) 1145.
[20] S.L. Yang, U. Krupp, H.J. Christ, V.B. Trindade, Advanced Engineering Materials 7 (2005) 723.
[21] Z.F. Zhang, Z.G. Wang, Materials Science and Engineering A (Structural Materials: Properties, Microstructure and Processing) A284 (2000) 285.
[22] W.T. Read, W. Shockley, Physical Review 78 (1950) 275.
[23] J.C.M. Li, Acta Metallurgica 8 (1960) 563.
[24] J.C.M. Li, B. Chalmers, Acta Metallurgica 11 (1963) 243.
[25] J.C.M. Li, Journal of Applied Physics 32 (1961) 525.
[26] D.G. Brandon, Acta Metallurgica 14 (1966) 1479.
[27] Y. Kaneko, K. Kitagawa, S. Hashimoto, Interface Science 7 (1999) 147.
[28] G. Palumbo, K.T. Aust, Acta Metallurgica et Materialia 38 (1990) 2343.
[29] M. Frary, C.A. Schuh, Acta Materialia 51 (2003) 3731.
[30] T. Watanabe, Res Mechanica: International Journal of Structural Mechanics and Materials Science 11 (1984) 47.
[31] T. Watanabe, Material Science Forum 46 (1989) 25–48.
[32] K.T. Aust, U. Erb, G. Palumbo, Materials Science and Engineering A A176 (1994) 329.
[33] L.S. Shvindlerman, G. Gottstein, Scripta Materialia 54 (2006) 1041.
[34] D.G. Brandon, B. Ralph, S. Ranganathan, M.S. Wald, Acta Metallurgica 12 (1964) 813.
[35] S. Ranganathan, Acta Crystallographica 21 (1966) 197.
[36] A.F. Acton, M. Bevis, Acta Crystallographica A (Crystal Physics, Diffraction, Theoretical and General Crystallography) A27 (1971) 175.
[37] A. Santoro, A.D. Mighell, Acta Crystallographica A (Crystal Physics, Diffraction, Theoretical and General Crystallography) A29 (1973) 169.
[38] H. Grimmer, W. Bollmann, D.H. Warrington, Acta Crystallographica A (Crystal Physics, Diffraction, Theoretical and General Crystallography) A30 (1974) 197.
[39] H. Grimmer, Acta Crystallographica A (Crystal Physics, Diffraction, Theoretical and General Crystallography) A30 (1974) 685.
[40] H. Grimmer, Acta Crystallographica A (Crystal Physics, Diffraction, Theoretical and General Crystallography) A32 (1976) 783.
[41] H. Grimmer, Acta Crystallographica A (Foundations of Crystallography) A40 (1984) 108.
[42] A.P. Sutton, V. Vitek, Philosophical Transactions of the Royal Society of London A (Mathematical and Physical Sciences) 309 (1983) 1.
[43] A.P. Sutton, V. Vitek, Philosophical Transactions of the Royal Society of London A (Mathematical and Physical Sciences) 309 (1983) 37.
[44] A.P. Sutton, V. Vitek, Philosophical Transactions of the Royal Society of London A (Mathematical and Physical Sciences) 309 (1983) 55.
[45] G.J. Wang, A.P. Sutton, V. Vitek, Acta Metallurgica 32 (1984) 1093.
[46] G. Wang, V. Vitek, Acta Metallurgica 34 (1986) 951.
[47] R.W. Balluffi, P.D. Bristowe, Surface Science 144 (1984) 28–43.
[48] V. Randle, Materials Characterization 47 (2001) 411.
[49] V. Randle, International Materials Reviews 49 (2004) 1.
[50] V. Randle, Acta Materialia 46 (1998) 1459.
[51] V. Randle, P. Davies, Interface Science 7 (1999) 5.
[52] V. Randle, Acta Crystallographica A (Foundations of Crystallography) A50 (1994) 588.
[53] V. Randle, Interface Science 10 (2002) 271.
[54] V. Randle, P. Davies, B. Hulm, Philosophical Magazine A (Physics of Condensed Matter: Structure, Defects and Mechanical Properties) 79 (1999) 305.
[55] D.M. Saylor, A. Morawiec, G.S. Rohrer, Acta Materialia 51 (2003) 3663.
[56] D.M. Saylor, B.S. El-Dasher, B.L. Adams, G.S. Rohrer, Metallurgical and Materials Transactions A (Physical Metallurgy and Materials Science) 35A (2004) 1981.
[57] G.S. Rohrer, B.S. El-Dasher, H.M. Miller, A.D. Rollett, D.M. Saylor, Proceedings of Materials Research Society, San Francisco, CA, United States, 2004, p. p265.
[58] J. Li, S.J. Dillon, G.S. Rohrer, Acta Materialia 57 (2009) 4304.
[59] Y. Bhandari, S. Sarkar, M. Groeber, M.D. Uchic, D.M. Dimiduk, S. Ghosh, Computational Materials Science 41 (2007) 222.
[60] S. Ghosh, Y. Bhandari, M. Groeber, Computer Aided Design 40 (2008) 293.
[61] D. Wolf, Acta Metallurgica 37 (1989) 1983.
[62] D. Wolf, Acta Metallurgica 37 (1989) 2823.
[63] D. Wolf, Acta Metallurgica et Materialia 38 (1990) 781.
[64] D. Wolf, Acta Metallurgica et Materialia 38 (1990) 791.
[65] J.D. Rittner, D.N. Seidman, Physical Review B (Condensed Matter) 54 (1996) 6999.
[66] D.L. Olmsted, S.M. Foiles, E.A. Holm, Acta Materialia 57 (2009) 3694.
[67] D.L. Olmsted, E.A. Holm, S.M. Foiles, Acta Materialia 57 (2009) 3704.
[68] Z. Otwinowski, W. Minor, in: C.W. Carter, R.M. SweetEd (Eds.), Macromolecular Crystallography, Academic Press, New York, 1997, pp. 307–326.
[69] J.J.L. Mulders, A. Gholinia, in: http://www.fei.com/uploadedFiles/Documents/Content/2006_06 (2006).
[70] S. Plimpton, Journal of Computational Physics 117 (1995) 1.
[71] S. Plimpton, Sandia National Laboratories, http://lammps.sandia.gov/, 2007.
[72] S.M. Foiles, J.J. Hoyt, Acta Materialia 54 (2006) 3351.
[73] D.J. Siegel, Applied Physics Letters 87 (2005) 121901.